ULTRASONIC IMAGING **27,** 221-236 (2005)

Soft tissue Absorption Tomography with Correction for Scattering Aberrations

EMILIE FRANCESCHINI,[1] MARIE-CHRISTINE PAUZIN,[1] SERGE MENSAH[1] AND JEAN-PHILIPPE GROBY[2]

[1]*Laboratoire de Mécanique et d'Acoustique – CNRS*
31 Chemin Joseph Aiguier
13402 Marseille Cedex 20 - France
franceschini@lma.cnrs-mrs.fr

[2]*Laboratory of Acoustics and Thermal Physics,*
Celestijnenlaan 200D, B-3001 Heverlee - Belgium

Among the many factors involved in ultrasound attenuation phenomena, scattering effects play a major role, even in the unexpected case of soft tissues. It is proposed in this study to quantitatively evaluate the scattering affecting the measurements before reconstructing the absorption parameter alone.

The reconstruction procedure involves three steps: (1) Estimating the sound speed map using a transmission tomography algorithm. This estimation procedure provides a numerical phantom of the organ probed, cleared of all dissipative components. This absorption free phantom mimics the (viscoacoustic) tissues imaged except for the density and absorption characteristics: the density *a priori* equals 1000 kg/m^3 and the absorption is not taken into account. The impedance fluctuations in the object are therefore approximated on the basis of the sound speed contrast. (2) Synthesing the field scattered by the absorption free phantom; the attenuation observed here results solely from the scattering phenomenon. The synthesis is carried out using a finite-element time domain code simulating the ultrasonic propagation through the phantom. It provides the scattering distortion reference introduced into the log spectral absorption estimator. (3) Reducing the scattering distortions affecting the integrated absorption measured along the ray paths using a log spectral procedure.

The corrected integrated absorption is then processed using a tomographic reconstruction procedure that provides an estimate of the absorption distribution. Simple numerical simulations show the improvement obtained in the absorption estimates with this approach.

Key words: Absorption tomography; scattering; viscoacoustic propagation model; ultrasound.

1. INTRODUCTION

During the past four decades, many clinical studies have suggested that a diagnostic imaging device sensitive to differences in the attenuation of tissues would be useful for improving detection and characterization procedures.[1-5] Several methods have been proposed for estimating ultrasound attenuation, which can be roughly subdivided into time domain[6-9] and frequency domain methods.[10-14] Although time-based techniques are generally easier to use than spectral techniques when making real time measurements, most authors have adopted a spectral approach.[15] Since tissue attenuation and beam diffraction are both frequency dependent, estimates obtained in the frequency domain tend to be more accurate and the results more consistent. Unfortunately, *in vivo* tissue attenuation measurements are difficult to per-

0161-7346/06 $18.00

form.[15] Ultrasound attenuation estimates are generally affected by many factors. Some of these factors, such as phase cancellation, transducer bandwidth, beam diffraction and focusing, which are system dependent, have been addressed using dedicated correction techniques.[16-21] Another important process, which is often underestimated as far as soft tissues are concerned, is the scattering induced by inhomogeneities,[21-23] which is one of the two main attenuation mechanisms at work in tissues, the other being the absorption by the medium due to dissipative processes. When dealing with inhomogeneous media, it is obviously rather difficult to separate the contributions of these two mechanisms. This is why the scattering has received little attention so far in the case of soft tissues, since the sound speed variations usually amount to less than 10%. In absorption transmission tomography studies, two simplifying assumptions are generally made. First, the diffraction(1) effects are ignored; this is equivalent to assuming that wave phenomena can be accounted for in terms of ray acoustics. The second assumption is that the propagation is rectilinear and that no refraction therefore occurs. Based on these hypotheses, the absorption images produced[25] are often spoiled by artefacts. Several research groups have attempted to correct for the refraction effects using iterative techniques based on numerical ray tracing methods[26] or an alternative approach using a perturbation analysis of refraction.[27] However, when the size of the inhomogeneities present in the object are of the same order of magnitude as the wavelength, the ray theory approach is no longer reliable.

The aim of the present study is to provide a means of accounting for the scattering effects from which standard absorption tomographic techniques suffer. The error introduced by the scattering in the log spectral difference method is evaluated and a scattering correction technique is proposed. Absorption reconstructions based on simulated data show the improvement obtained using this method.

2. SCATTERING EFFECTS IN ULTRASOUND ABSORPTION ESTIMATION

In order to describe the scattering effects induced by the inhomogeneities present in the medium, we assume that the ultrasound device is a linear system and, within the narrow bandwidth usually used in ultrasound methods, that the tissue absorption increases linearly with the frequency:[28] $(\underline{x},f) = {}_0(\underline{x})\, f$. f is the frequency in Hz; $(\underline{x},f)$ is the frequency dependent absorption coefficient of the tissue at any point $\underline{x}$ on a cross-sectional plane. ${}_0(\underline{x})$ is the absorption coefficient of linear frequency dependence (in $Np.cm^{-1}.MHz^{-1}$). A similar analysis of the scattering effects on the insertion log spectral difference technique has been proposed by Xu and Kaufman,[21] who took into consideration the transducer diffraction induced distortion. Here it is proposed to focus on the scattering due to the heterogeneities present in the medium.

Let us consider two transducers, one transmitter and one receiver placed in a water tank and make two measurements: one with and one without the tissue placed between the transducers. The amplitude spectrum $Y_w(f)$ of the ultrasound signal propagating through the water (reference signal) equals:

$$\left|Y_w(f)\right| \quad \left|Y_0(f)\; H_w(f)\right| \tag{1}$$

where $Y_w(f)$ is the Fourier transform of the recorded signal $y_w(t)$ defined by $Y_w(f) = y_w(t)e^{-j2\pi ft}dt$. $Y_0(f)$ is the spectral instrumental function, which includes the amplitude spectrum of the electrical input signal and the transfer functions of the transmitting and re-

(1) Diffraction corresponds here to wave processes that cannot be accounted for in terms of ray acoustics. On the other hand, scattering refers to all reflection processes, whether specular or not.[24]

ceiving transducers. $H_w(f)$ characterizes the effects of the scattering on the ultrasound pulse along the water path alone, corresponding to the transducer diffraction.

The amplitude spectrum $Y_{mes}(f)$ of the signal recorded with the tissue inserted corresponds to:

$$\left|Y_{mes}(f)\right| \quad \left|Y_0(f)H_w(f)H_{sc}(f)\right| e^{-\left(\int_{ray} {}_0(\underline{x})ds\right)f} \tag{2}$$

where $H_{sc}(f)$ characterizes the effects of the scattering processes on the ultrasound pulse along the water-tissue-water propagation path.

Log spectral difference technique

The linear model described above is generally written in the case of a homogeneous layer of tissue probed by a plane wave so that the interfaces encountered are perpendicular to the beam; only absorption occurs in this case. The integrated absorption $A_w(f)$ is the slope of the log spectral ratio $Y_w(f)/Y_{mes}(f)$ versus the frequency f[10]:

$$A_w(f) \quad \int_{ray} {}_{0w}(\underline{x})ds \quad \frac{\ln\left|Y_w(f)\right| \quad \ln\left|Y_{mes}(f)\right|}{f} \tag{3}$$

where ${}_{0w}$ is the absorption coefficient estimated when the scattering effects are neglected. This technique is no longer relevant when ultrasonic absorption tomography is performed on complex tissue structures where the interfaces are not necessarily perpendicular to the beam. The lack of scattering considerations will inevitably result in large errors in the estimated absorption coefficient. Instead of using Eq. (3), the integrated absorption coefficient $A(f)$ is derived from Eq. (2):

$$A(f) \quad \int_{ray} {}_0(\underline{x})ds \quad \frac{\ln\left|Y_w(f)\right| \quad \ln\left|Y_{mes}(f)\right| \quad \ln\left|H_{sc}(f)\right|}{f}. \tag{4}$$

The error introduced when Eq. (3) is used instead of Eq. (4) is the scattering induced distortion $D(f)$:

$$D(f) \quad \int_{ray} {}_0(\underline{x}) \quad {}_{0w}(\underline{x}) \; ds \quad \frac{\ln\left|H_{sc}(f)\right|}{f}. \tag{5}$$

3. CORRECTION FOR SCATTERING EFFECTS

It is now proposed to separate the scattering and dissipative mechanisms that contribute to the attenuation phenomenon by estimating $D(f)$ and then calculating $A(f)=A_w(f)+D(f)$.

For this purpose, we will attempt to predict the field scattered by the organ. In the first step, in order to obtain a rough approximation of the scattering processes, we reconstruct the velocity map of the object investigated. This velocity map is associated with a constant density map (1,000 kg/m^3) and a null attenuation map in order to build up a dissipation free acoustical model that we have named the *numerical phantom* or simply the *phantom*. We simulate ultrasonic wave propagation through this phantom using a finite element time domain propagation code.

The amplitude spectrum $Y_{sim}(f)$ of the pulse recorded after the simulated wave propagation through the phantom (inserted between the two transducers) is given by:

$$\left|Y_{sim}(f)\right| \quad \left|Y_0(f)H_w(f)\widetilde{H}_{sc}(f)\right| \tag{6}$$

where $\widetilde{H}_{sc}(f)$ characterizes the effects of the scattering on the ultrasound pulse along the water-phantom-water propagation path. Similar spectra are obtained in the absence of the phantom (water reference $Y_w(f)$). The scattering induced distortion is then estimated by:

$$\widetilde{D}(f) \quad \frac{\ln\left|\widetilde{H}_{sc}(f)\right|}{f} \quad \frac{\ln\left|Y_{sim}(f)\right| \quad \ln\left|Y_w(f)\right|}{f} \tag{7}$$

and is removed from the water-reference integrated absorption $A_w(f)$ in order to obtain the estimated integrated absorption:

$$\widetilde{A}(f) \quad \underset{ray}{\sim}_0(\underline{x})\,ds \quad A_w(f) \quad \widetilde{D}(f) \quad \frac{\ln\left|Y_{sim}(f)\right| \quad \ln\left|Y_{mes}(f)\right|}{f}. \tag{8}$$

The integrated absorption is therefore given by the slope of the log spectral ratio $Y_{sim}(f)/Y_{mes}(f)$ versus the frequency f. Lastly, a transmission tomographic procedure is used to determine the estimated absorption distribution.

For this correction method to work, the scattering effects have to be fairly similar in both the tissue sample and numerical phantom so that the relation is acceptable. The sound speed, density and absorption fluctuations all contribute to the scattering effects. In practice, the density map is not known and in order to overcome the fact that the parameter distributions are difficult to observe, we assume that the object has a constant density equal to 1,000 kg/m^3. In the case of adipose tissues, this will be an overestimate and in that of muscle and stroma tissues, it will be an underestimate. The impedance fluctuations are therefore approximated by the sound speed variations.

4. APPLICATION TO SIMULATED DATA

In order to assess the scattering correction procedure, we consider a numerical tissue-like model (Fig. 1) whose scattering response is computed using a Finite Element time domain Method (FEM). This method has been extended to include absorption-dispersion effects.[29,30] The governing numerical expressions on which the FEM is based can be found in appendix A. A grid consisting of 1730 × 1730 pixels = 0.016 mm, 27.7 mm × 27.7 mm) is used. The ring antenna, which is composed of 360 equally-spaced transducers (point-like transmitters and receivers, central frequency 2.5 MHz, = 0.6 mm), has a radius of R = mm Each transducer emits a short pulse while the remaining elements act as receivers. The temporal and spectral plots of the transmitted pulses are shown in figure 2. The academic cylindrical model, which is immersed in water (density 1,000 kg/m^3, velocity 1,500 m/s), simulates a fluid object having the following characteristics: density 950 kg/m^3, velocity 1,470 m/s (without any dissipative considerations) and absorption 6 Np/m/MHz. The external radius of the cylinder is 11 mm. The diameters of the inclusions are d_0 = 8 = 3.6 mm, d_1 =

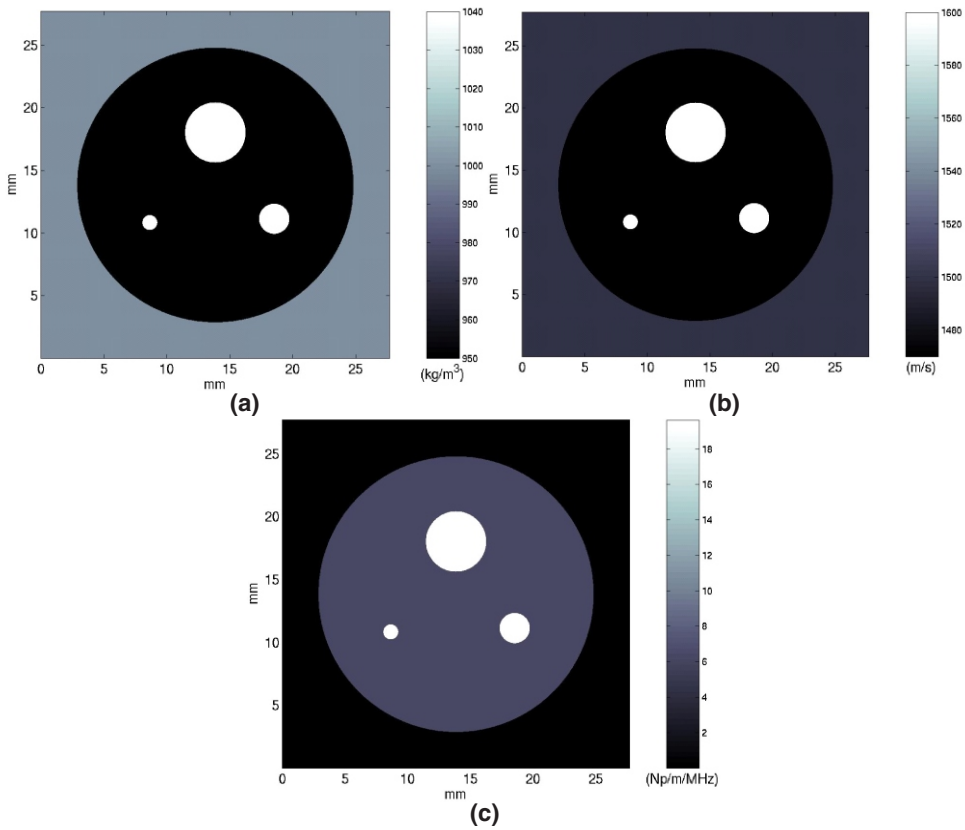

FIG. 1 Cylindrical academic computer phantom. (a) Density map, (b) sound speed map and (c) absorption map.

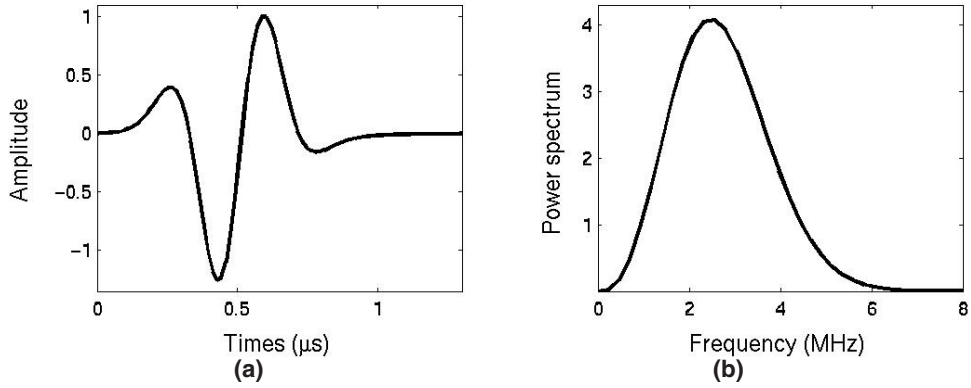

FIG. 2 2.5 MHz cylindrical wave used in the FEM simulations in (a) time and (b) frequency.

4 =2.4 mm and d_2= 2 =1.2 mm. The inclusions have the following characteristics: density 1,060 kg/m^3, velocity 1,600 m/s (without any dissipative considerations) and absorption 19 Np/m/MHz. Figure 3 shows the variations *(f)/f* as a function of *f* obtained with the viscoacoustic code (based on the imaginary part of Eq. (A2) in appendix A). One can observe here that the simulated absorption *(f)* is almost linear with the frequency in the case of both tissues.

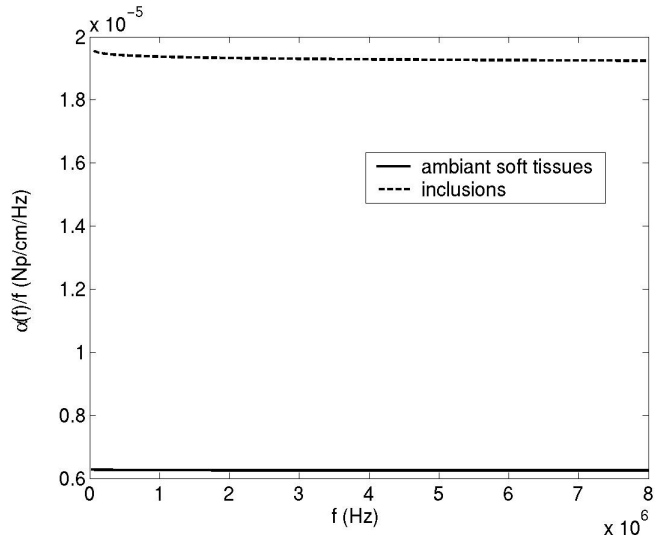

FIG. 3 (*f*)/(*f*) as a function of *f*.

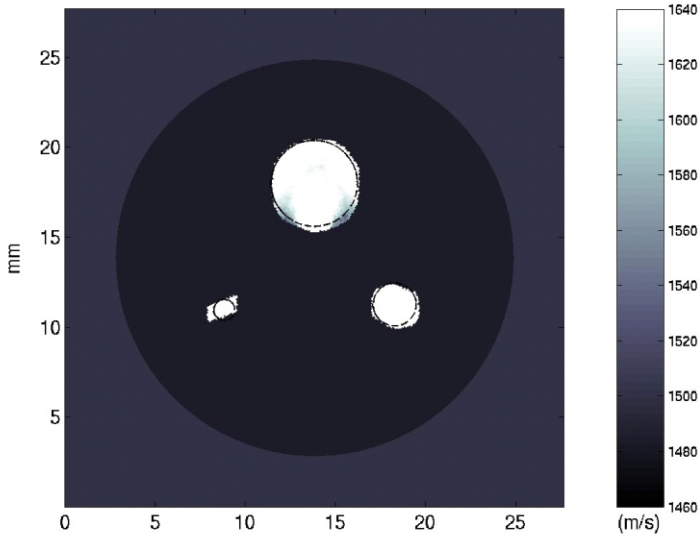

FIG. 4 Reconstruction of the sound speed via the layer stripping technique.

Figure 4 illustrates the velocity map reconstructed using the layer stripping technique[31, 32] presented in appendix B. The average estimate of the inclusion sound speed is 1,634 m/s and the standard deviation is 15%, which corresponds to the dispersion curves given in figure 5. In the case of the inclusions, the dispersion (Fig. 5) induces sound speed changes in the 20 m/s to 30 m/s range in the 1.5-4 MHz frequency bandwidth.

Ultrasound propagation was simulated through the estimated absorption free phantom having the velocity map shown in figure 4 and the scattering correction procedure was applied. We must point out that we have regularized the inclusions borders (the inclusions were given the shape of regular ellipses) in order to prevent irregularities in shape from increasing the scattering phenomenon. Tomographic reconstructions were performed using the fan beam algorithm described by Kak and Slaney.[33] 360 projections taken over an angle

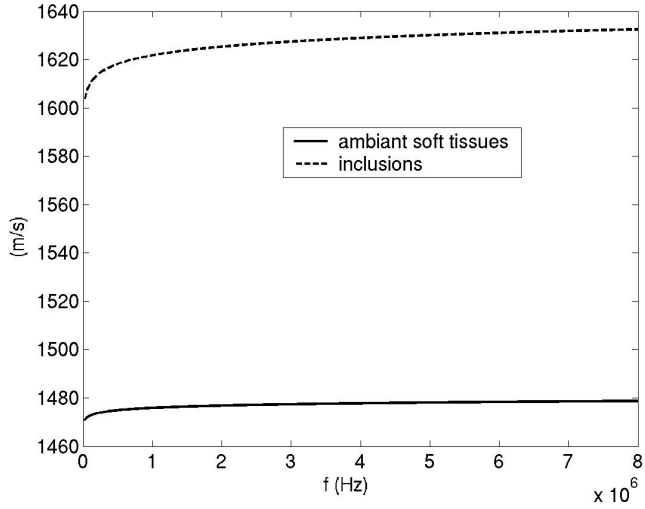

FIG. 5 Evolution of the sound speed versus *f*.

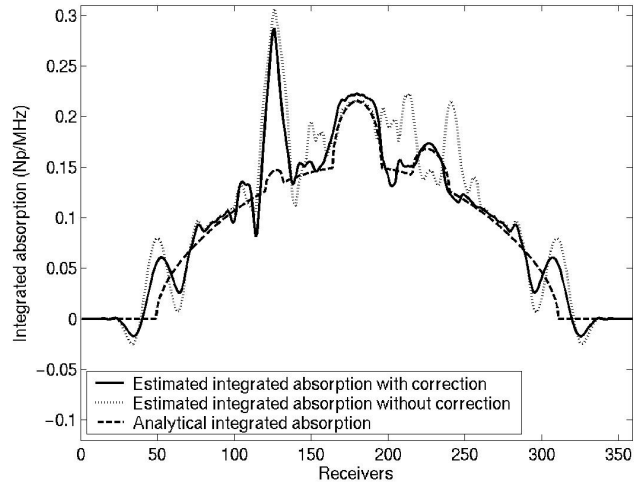

FIG. 6 Projection data for one transmitter ($x = 0.65$ mm, $y = 13.85$ mm) using log spectra difference method with and without correction of the scattering effects.

of 360° in transmission were used. In figure 6, in the case of a given transmitter ($x = 0.65$ mm, $y = 13.85$ mm), the projection data of the analytical integrated absorption and the estimated integrated absorption (obtained with the simulated data) are compared. At receivers 90° to 270° (those used in transmission tomography), the absorption estimates were greatly improved, especially in the case of the two largest inclusions 8 and 4 in diameter. In the case of these two inclusions, the maximum relative error was 53% without correcting and 7% after correcting for the scattering effects.

Figures 7 and 8 show the reconstructions obtained when the integrated absorption was calculated neglecting the scattering effects, as in Eq. (3), after correcting for the scattering effects, as done in Eq. (8), respectively. In the case of the classical reconstruction method (Fig.

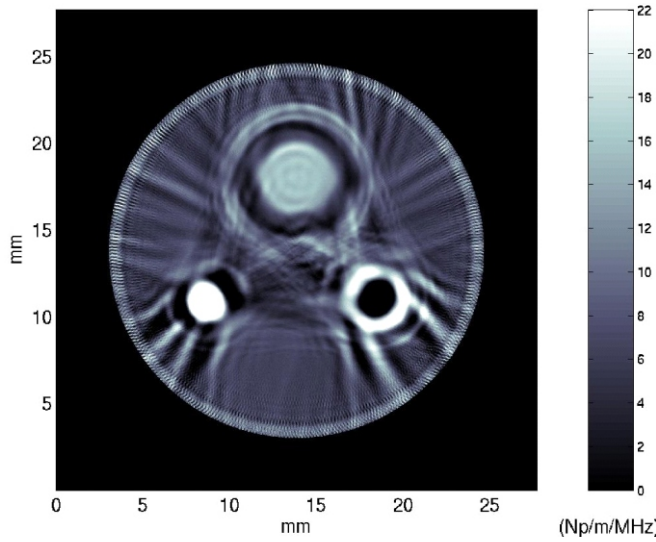

FIG. 7 Reconstruction using the classical log spectra difference technique.

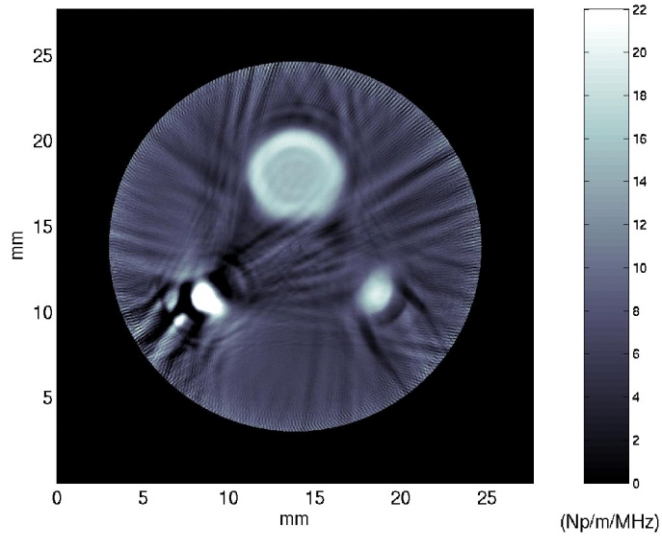

FIG. 8 Reconstruction using log spectral difference technique with correction for the scattering effects.

7), one can note the artifacts (concentric circles) around the two biggest inclusions. Figure 9 gives the corresponding line profiles of both reconstructions. Both reconstructions with and without correction for the scattering effects show that with both methods, objects of twice the wavelength can be detected. Scattering correction makes it possible to discriminate the size and to evaluate the absorption of objects of four times the wavelength (Fig. 8). In the case of the smallest inclusions, neither of these methods of reconstruction was satisfactory, however. The errors were mainly due to the poor delimitation of the smallest inclusion in the sound speed map reconstruction (Fig. 4). Figure 10 shows the tomographic reconstruction obtained when the correction was performed with a sound speed map drawn up with real size objects and the average sound speeds obtained via the layer stripping method (ambient soft tissues 1,480 m/s and inclusions 1,634 m/s). This greatly improved the absorption estimate

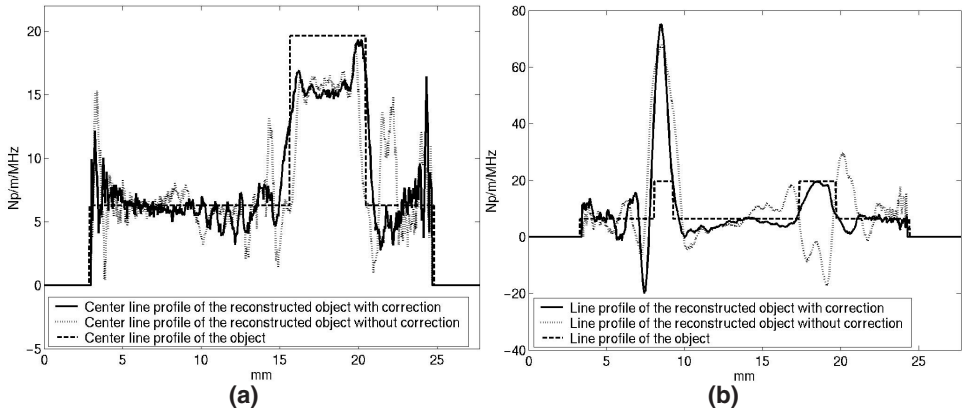

FIG. 9 Comparisons of the line profiles of the reconstructed object without (plotted line) and with (continuous line) correction of the scattering effects.

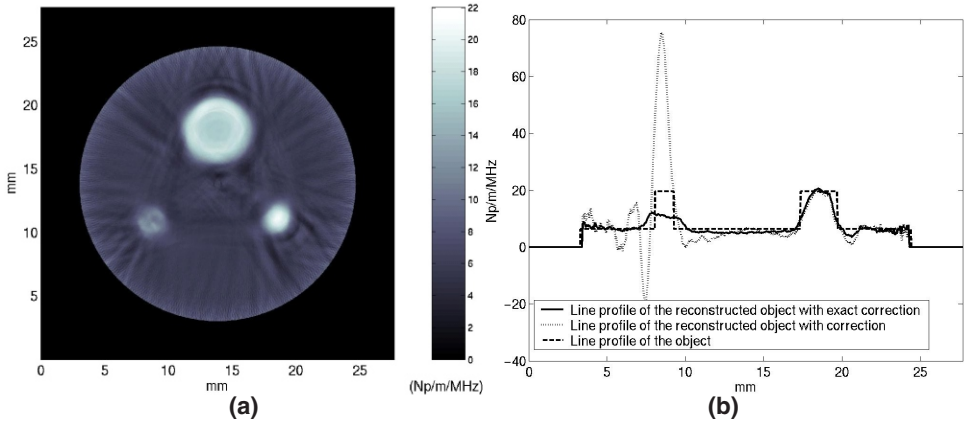

FIG. 10 Reconstruction using log spectral difference technique with exact correction of the scattering effects (a) and line profile (b).

of the smallest inclusions. The weakest point of this method is therefore the fact that it is sensitive to the discrimination of the inclusions of the same order of size as the wavelength (resonance phenomenon).

In conclusion, ultrasound scattering errors due to sound propagation occurring in inhomogeneous media blur the image and induce strong artifacts, especially if the size of the heterogeneities is of the same order as the wavelength. The reconstructions based on simulated data presented here show how applying scattering correction to the overall absorption estimates can improve the results obtained.

5. CONCLUSION

The artifacts observed in the tomographic reconstructions obtained using the classical log spectral difference technique have been mostly due to the fact that the scattering processes have been neglected. In order to overcome this problem, we have developed a method for estimating the scattering. Since this process results mainly from the propagation perturbations due to sound speed contrasts, a sound speed map was first reconstructed. This numerical

model provided the input material for a time-domain finite element code simulating the wave propagation. This absorption free phantom mimics the tissues (viscous fluid) imaged except for the density and absorption characteristics: the density is taken *a priori* to be 1,000 kg/m^3, and the absorption is not taken into account. The impedance fluctuations in the object are therefore approximated in terms of the estimated sound speed contrast. This realistic numerical model can be used to predict the scattered field without any absorption interference and this field constitutes our scattering distortion reference field in the log spectral difference absorption estimates. A tomographic procedure was used to reconstruct an absorption map of the tissue under investigation. Numerical simulations illustrate the results obtained at each step and comparisons show the improvement obtained in the absorption contrast estimates. These results show that even in the case of small speed variations (1,470 m/s – 1,600 m/s), the effects of the scattering are non-negligible and can greatly degrade the quality of absorption tomographic images.

In practical situations, the method used here to correct the experimental data may not be as efficient as with simulated signals. In this study, the simulated dissipative data to be corrected and the simulated nondissipative data used for the correction were generated from two versions of the same propagation code. This situation will differ in experimental contexts, where the waves undergo all the propagation effects (3D, non linearity, etc). In addition, in practical situations, the active transducers are all distinct, not point sources and have their own directivity index. Theoretically, this should not greatly affect the absorption measurements, but in practice, 'calibration' and 'spatial deconvolution' are known to be rather delicate processes.

In conclusion, the numerical computations presented here show that the scattering cannot be overlooked (even in soft tissues) when ultrasound absorption is evaluated using insertion techniques. The absorption tomographic reconstructions carried out here show the improvement that can be achieved using the method described. In the case of high contrast objects, current approaches that operate on phase estimates could be associated with this method to improve the velocity dispersion estimation.

ACKNOWLEDGEMENTS

This study was supported by Ville de Marseille, Région Provence-Alpes-Cote d'Azur, Conseil Général 13 and CNRS-LMA. The authors thank the Institute for Development and Resources in Intensive Scientific computing (IDRIS) where a some of the computations were performed. We are grateful to Chrysoula Tsogka (researcher at CNRS) for putting her propagation code at our disposal and Laurent Pruvost (EGIM) for his participation in the attenuation estimation procedure.

APPENDIX A

Finite element method

Real media, such as soft tissues, disperse and attenuate the waves. The propagation of an acoustic wave in a medium of this kind occupying a domain can be modelled by the following system:

$$P_t \qquad \begin{array}{lll} \underline{x}\ \dfrac{\underline{v}\ \underline{x},t}{t} & p\ \underline{x},t & \text{in} \quad]0,T] \\ p\ \underline{x},t \quad (\underline{x},t)_t & .\underline{u}(\underline{x},t) & \text{in} \quad]0,T] \end{array} \tag{A1}$$

where the unknowns are the particular velocity $\underline{v}(\underline{x},t)$, the displacement $\underline{u}(\underline{x},t)$ such that $\underline{v}(\underline{x},t)= \underline{u}(\underline{x},t)/ t$, and the pressure $p(\underline{x},t)$, and the data are the density $(\underline{x})$ and the visco-acoustic modulus $(\underline{x},t)$, which depends on time. $_t$ depicts the convolution product. As proposed in numerical studies,[29, 30] one may note that the pressure in the first equation of the system Eq. (A1) is the opposite of the usual pressure.

A dissipative medium can be described by either of two quantities: either by the quality factor

$$Q^{1} \left| \frac{\underline{x},}{\underline{x},} \right|$$

or by the attenuation $( )$ defined as the imaginary part of the wave number $k( )$. Soft tissues are often described by[28] $( )=$, where is typically approximately equal to 1. We have established that this behaviour corresponds to a constant quality factor within a frequency band.[29, 30] Using Kjartansson's formulae[34] and adopting this assumption, the wave number takes the following form:

$$k \quad \frac{}{c_{ref}} \frac{i}{_{ref}} \quad ^{\frac{1}{}\arctan \frac{1}{Q}} \tag{A2}$$

where c_{ref} is the velocity at the reference frequency $_{ref}$.

The second equation (i.e., the constitutive equation) of the system Eq. (A1) is of no practical use in a time domain finite element method because it requires storing in memorythe whole history of the unknowns in order to perform the convolution product. The most usual way of avoiding this problem is to approximate the viscoacoustic modulus in the frequency domain by a low order frequency rational function.[29, 30, 35-37] In what follows, for the sake of convenience, we introduce the relaxation function $R(\underline{x},t)$, defined by:

$$\underline{x}, \quad \frac{R(\underline{x},t)}{t}; \; R(\underline{x},t) \quad _R(\underline{x}) \quad (\underline{x}) \quad _0 r(x, \; ')e^{\; '}d \; ' \; H(t), \tag{A3}$$

where $_R(\underline{x})=lim\ t \quad R(\underline{x},t)$ is the relaxed modulus, $_U(\underline{x})= \; _R(\underline{x})+ \quad (\underline{x})=lim\ t \quad 0\, R(\underline{x},t)$ the unrelaxed modulus, $r(\underline{x}, \;)$ the normalized relaxation spectrum and $H(t)$ the Heaviside function. Substituting into the second equation of Eq. (A1) gives

$$p(\underline{x},t) \quad _U(\underline{x}) \quad . \underline{u}(\underline{x},t) \quad (\underline{x}) \quad ^{t} \quad _0 \; 'r(\underline{x}, \; ')e^{\; '(t \;)} \; . \underline{u}(\underline{x}, \;)d \; 'd \; . \tag{A4}$$

We now assume that the relaxation spectrum can be approximated by L single peaks of amplitude $_l$ at relaxation frequencies $_l$:

$$r(\underline{x}, \;) \quad _{l \; 1}^{L} \quad _l(\underline{x}) \quad _l(\underline{x}) \; ; \quad _{l \; 1}^{L} \quad _l(\underline{x}) \; 1 \; . \tag{A5}$$

We get

$$R(\underline{x},t) \quad _R(\underline{x}) \quad (\underline{x}) \quad _{l \; 1}^{L} \quad _l(\underline{x})e^{\; _l(\underline{x})t} \quad H(t), \tag{A6}$$

and

$$ _L \underline{x}, \qquad _R(\underline{x}) \; 1 \quad \sum_{l\,1}^{L} \frac{i \quad y_l(\underline{x})}{i \qquad _l(\underline{x})} \quad . \tag{A7} $$

In Eq. (A6), we introduced $y_l(\underline{x})$ defined by

$$ y_l \; \underline{x} \quad \frac{(\underline{x})}{_R(\underline{x})} \quad _l(\underline{x}) \; , \tag{A8} $$

with

$$ \sum_{l\,1}^{L} y_l(\underline{x}) \quad \frac{(\underline{x})}{_R(\underline{x})}. $$

The relaxation frequencies $_l$ are taken to be equidistant on a logarithmic scale between $_{max}/100;\ _{max}$, where $_{max}$ is the maximum frequency of the spectrum of the source used in the numerical simulation while the weights $y_l(\underline{x})$ are obtained by solving the overdetermined system obtained by equalizing the approximated inverse of the quality factor with its nonapproximated value at $2L+1$ frequencies.

After substituting into the constitutive equation, this can be rewritten in the form of two coupled equations

$$ \begin{aligned} & i \quad p(\underline{x}, \quad) \; i \quad \sum_{l\,1}^{L} \quad _l \; \underline{x}, \qquad _R \; \underline{x} \quad .\underline{v} \; \underline{x}, t \\ & i \quad _l \; x, \qquad _l \; \underline{x} \quad _l \; \underline{x}, \qquad y_l(\underline{x}) \quad _R \; \underline{x} \quad .\underline{v} \; \underline{x}, t \end{aligned} \tag{A9} $$

where $_l(\underline{x}, \quad)$ are the memory variables. Back in the time domain, together with the conservation of the momentum, the final system takes the form of three first order in time coupled equations:

$$ P_t \quad \begin{aligned} & \frac{\underline{v} \; \underline{x}, t}{t} \qquad p(\underline{x}, t) \quad \text{in} \quad]0; T] \\ & \frac{p(\underline{x}, t)}{t} \quad \sum_{l\,1}^{L} \quad \frac{_l \; \underline{x}, t}{t} \qquad _R \; \underline{x} \quad .\underline{v} \; \underline{x}, t \quad \text{in} \quad]0; T] \\ & \frac{_l \; \underline{x}, t}{t} \qquad _l(\underline{x}) \quad _l \; \underline{x}, t \quad y_l(\underline{x}) \quad _R \; \underline{x} \quad .\underline{v} \; \underline{x}, t \quad \text{in} \quad]0; T] \end{aligned} \tag{A10} $$

For the space discretization, we use a mixed finite-element method[38] and for the discretization in time, we employ a second order-centered finite difference scheme. The simulation grid is surrounded by an absorbing layer (PML) simulating unbounded domains.[39] Further details of the numerical method used can be found in references 29 and 30.

APPENDIX B

Layer stripping procedure

Based on the time of flight (TOF) elapsing between the transmitter and the receiver, the layer stripping technique consists in recovering the velocity map of the medium step by step,

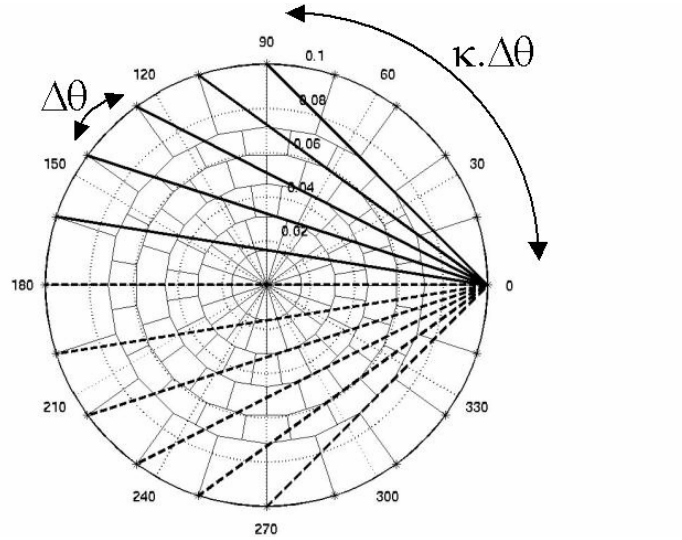

FIG. 11 Acquisition configuration in transmission.

working from the external layer to the innermost one. For this purpose, a cylindrical mesh grid of concentric layers of cells is built. The numbers of layers and cells depend on the number N of transducers uniformly distributed over a circle around the breast N, as well as on the minimum angle at which the data are acquired in transmission. The cylindrical mesh is then composed of $N_l = N/2$ - layers, and N cells/layer (Fig. 11).

The layer stripping algorithm is as follows:

Let us note $M(i,j)$ the cell sited in layer i ($i = 1,.,N_l$) within the angular limits [$(j-1)$ j ($j = 1, .,N$). We define $D(i)$ the transducer located at the angular position (i-1) and n,m the ray between the transmitter $D(n)$ and the receiver $D(m)$. We write the length $L\ i,j,n,m$ of that ray within the cell $M\ i,j$ as follows: $L\ i, j, n, m$ $n, m\ dl$.

$M\ i,j$

We call $_{i,j}$ the set of rays crossing the same cell (Fig. 12),

$$C_{i,j} \quad \frac{1}{\quad} \qquad n,m \quad c\ n,m$$

$_{i,j}$ n,m $_{i,j}$

Assuming that the sound speed values of the cells are known in the external layers $l < i$, the sound speed estimator $C_{i,j}$ of the cell $M\ i,j$ is given by:

$$c\ n,m \quad \frac{i,n,m}{t\ n,m \qquad t_l\ n,m} \tag{A12}$$

$1\ l\ i$

where $c\ n,m$ is the averaged speed of sound calculated from the TOF along n,m and corrected from the estimates already made on the adjacent external layers using the procedure described below:

Let us call $t(n, m)$ the travel time of the wave propagating from $D(n)$ to $D(m)$ and $t_l(n,m)$, 1 l i, the travel time of that wave within the external layers, then

$$c\ n,m \quad \frac{i,n,m}{t\ n,m \qquad t_l\ n,m} \tag{A12}$$

$1\ l\ i$

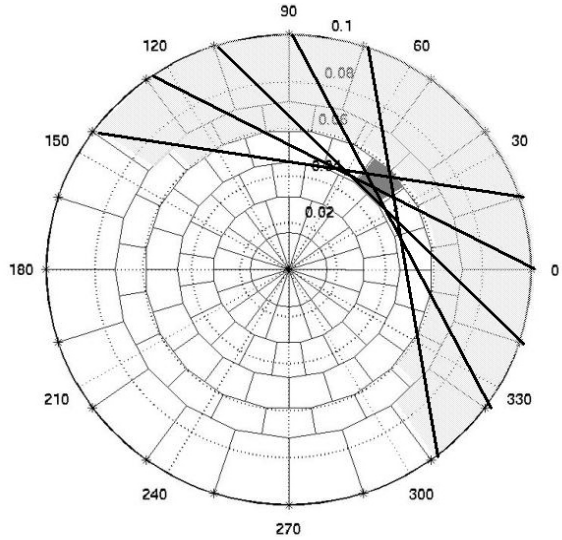

FIG. 12 Layer-stripping principle.

where (i,n,m) stands for the length of the ray in layer i.

The antenna is composed here of 360 transducers. The minimum angle at which the data are acquired in transmission tomography equals 33° and the cylindrical mesh is composed of 148 layers. The reconstruction is carried out in two steps:

1. A first scan (using the transducer configuration shown in figure 11) is performed in order to determine the host medium sound speed. The result is a binary sound speed map demarcating the host medium and the inclusions of variable sound speeds that have to be determined,
2. The layer stripping technique (Fig. 12) is then used to determine the sound speeds of the inclusion.

REFERENCES

1. McDaniel G. Ultrasonic attenuation measurements on excised breast carcinoma at frequencies from 6 to 10 MHz, in *Proc IEEE Ultrasonics Symp,* pp. 234-23 *(*IEEE Cat. no. 77CH1264-ISU, 1977).

2. Fry EK, Sanghi N, Fry F, Gallager H. Frequency dependent attenuation of malignant breast tumors studied by the fast Fourier transform technique, in *Ultrasound Tissue Characterization II,* Linzer M, ed., pp. 85-92, NBS Special Publication 525 (US Government Printing Office, 1979).

3. Kuc R. Clinical application of an ultrasound attenuation coefficient estimation technique for liver pathology characterization, *IEEE Trans Biomed Eng 27* 312-319 (1980).

4. Maklad NF, Ophir J, Balsara V. Attenuation of ultrasound in normal liver and diffuse liver disease in vivo, *Ultrasonic Imaging 6*, 117-125 (1984).

5. Landini L, Sarnelli R, Squantini F. Frequency-dependent attenuation in breast tissue characterization, *Ultrasound Med Biol 11*, 599-603 (1985).

6. Flax SW, Pelc NJ, Glover GH, Gutmann FD, McLachlan M. Spectral characterization and attenuation measurements in ultrasound, *Ultrasonic Imaging 5*, 95-116 (1983).

7. Claesson I, Salomonsson G. Estimation of varying ultrasonic attenuation, *Ultrasound Med Biol 11*, 131-145 (1985).

8. He P, Greenleaf JF. Application of stochastic analysis to ultrasonic echoes - Estimation of attenuation and tissue heterogeneity from peaks of echo envelope, *J Acoust Soc Am 79*, 526-534 (1986).

9. Jiang HS, Song TK, Park SB. Ultrasound attenuation estimation in soft tissue using the entropy difference of pulsed echoes between two adjacent envelope segments, *Ultrasonic Imaging 10*, 248-264 (1988).

10. Kuc R, Schwartz M. Estimating the acoustic attenuation coefficient slope for liver from reflected ultrasound signals, *IEEE Trans Sonics Ultrasonics SU-26*, 353-362 (1979).

11. Meyer CR. An iterative, parametric spectral estimation technique for high-resolution pulse-echo ultrasound, *IEEE Trans Biomed Eng 26*, 207-212 (1979).

12. Dines KA, Kak AC. Ultrasonic attenuation tomography of soft tissues, *Ultrasonic Imaging 1*, 16-33 (1979).

13. Narayana PA, Ophir J. Spectral shifts of ultrasonic propagation: A study of theorotical and experimental models, *Ultrasonic Imaging 5*, 22-29 (1983).

14. Fink M, Hottier F, Cardoso JF. Ultrasonic signal processing for in vivo attenuation measurement: short time fourier analysis, *Ultrasonic Imaging 5*, 117-135 (1983).

15. Ophir J, Shawker TH, Maklad NF et al. Attenuation estimation in reflection: progress and prospects, *Ultrasonic Imaging 6*, 349-395 (1984).

16. Pan KM, Liu CN. Tomographic reconstruction of ultrasonic attenuation with correction for refractive errors, *IBM J Res Develop 25*, 71-82 (1981).

17. Cloostermans MJ, Thijssen JM. A beam corrected estimation of the frequency dependent attenuation of biological tissues from backscattered ultrasound, *Ultrasonic Imaging 5*, 136-147 (1983).

18. Insana M, Zagzebski J, Madsen E. Improvements in the spectral difference method for measuring ultrasonic attenuation, *Ultrasonic Imaging 5*, 331-345 (1983).

19. O'Donnell M. Effects of diffraction on measurements of the frequency dependent ultrasonic attenuation, *IEEE Trans Biom Engin 30*, 320-326 (1983).

20. Laugier P, Berger G, Fink M, Perrin J. Diffraction correction for focused transducers in attenuation measurements in vivo, *Ultrasonic Imaging 9*, 258-259 (1987).

21. Xu W, Kaufman JK. Diffraction correction methods for insertion ultrasound attenuation estimation, *IEEE Trans Biom Eng 40*, 563-570 (1993).

22. Sehgal CM, Greenleaf JF. Scattering of ultrasound by tissues, *Ultrasonic Imaging 6*, 60-80 (1984).

23. Laugier P, Berger G, Fink M, Perrin J. Specular reflector noise: effect and correction for in vivo attenuation estimation, *Ultrasonic Imaging 7*, 277-292 (1985).

24. Morfey CL. *Dictionary of Acoustics* (Academic Press, pp. 110, 2001).

25. Greenleaf JF, Johnson SA, Lee SL, Herman GT, Wood EH. Algebraic reconstruction of spatial distributions of acoustic absorption within tissue from their two dimensional acoustic projections, in *Acoustical Holography 5*, pp. 591-603 (Plenum Press, New York, 1974).

26. Johnson SA, Greenleaf JF, Samayoa WF, Duck FA, Sjosstrand JD. Reconstruction of three-dimensional velocity fields and others parameters by acoustic ray tracing, in *Proc IEEE Ultrasonics Symp*, pp. 46-51 (1975).

27. Norton SJ, Linzer M. Correcting for ray refraction in velocity and attenuation tomography: a perturbation approach, *Ultrasonic imaging 4*, 201-233 (1982).

28. Sehgal C, Greenleaf JF. Ultrasonic absorption and dispersion in biological media: a postulated model, *J Acoust Soc Am 72*, 1711-1718 (1982).

29. Groby JP, Tsogka C. A time domain method for modeling wave propagation phenomena in viscoacoustic media, in *Proc 6th Inter Conf on Maths Num Aspects Wave Propag*., pp. 911-915 (2003).

30. Groby JP, Tsogka C. A time domain method for modeling viscoacoustic wave propagation, *J Comput Acoust* (in press, 2005).

31. Ferriere R, Mensah S. Weakly inhomogeneous media tomography, *Ultrasonic Imaging 25*, 122-133 (2003).

32. Mensah S, Ferriere R. Diffraction tomography: a geometrical distortion free procedure, *Ultrasonics 42*, 677-682 (2004).

33. Kak AC, Slaney M. *Principles of computerized Tomographic Imaging,* pp. 77-86 (IEEE Press, New York, 1988).

34. Kjartansson E. Constant Q wave propagation and attenuation, *J Geophys Roy 8*4, 4737-4748 (1979).

35. Emmerich H, Korn M. Incorporation of attenuation into time-domain computations of sismic wave fields, *Geophysics 52*, 1252-1264 (1987).

36. Day SM, Minster JB. Numerical simulation of attenuated wavefield using a Padé approximant method, *Geophys J Roy Astr Soc 78*, 105-118 (1984).

37. Robertson JAO, Blanch JO, Symes WW. Modeling of a Q constant: methodology and algorithm for an efficient and optimally inexpensive viscoelastic technique, *Geophysics 60*, 178-184 (1995).

38. Bécache E, Joly P, Tsogka C. An analysis of new mixed finite elements for the approximation of wave propagation problems, *SIAM J Numer Anal 37*, 1053-1085 (2000).

39. Collino F, Tsogka C. Application of the pml absorbing layer model to the linear elastodynamic problem in anisotropic heteregeous media, *Geophysics 66*, 294-305 (2001).